

Supplementary Information for
Foamed Silicon Particle as a High Capacity Anode Material for
Lithium-ion Battery

Myungbeom Sohn, Hyeong-Il Park, Hansu Kim*

Department of Energy Engineering, Hanyang University, Seoul 04763, Republic of Korea

***Corresponding author**

E-mail: khansu@hanyang.ac.kr

Tel: +82-2-2220-2414

Fax: +82-2-2220-2489

Experimental Section

Materials preparation: Commercial bulk Si powder (-325 mesh, 99% trace metals basis) was purchased from Sigma-Aldrich. Ball-milled Si powder was obtained by ball milling of the bulk Si powder for 36 h at 1000 rpm with a ball-to-powder ratio of 20:1 under an argon (Ar) atmosphere at room temperature using a custom-made vibratory mill. Foamed Si powder was prepared by wet alkaline chemical etching of the ball-milled Si using the following method. First, 0.3 g of ball-milled Si powder was dispersed in 60 mL of deionized water by ultrasonic agitation for 30 min using an ultrasonic bath (Branson CPX3800H-E). To etch the ball-milled Si, ultra-sonication was carried out on a solution of ball-milled Si dispersed in 40 mL of 0.5 M sodium hydroxide (NaOH) solution in a polypropylene bottle. To quench the etching reaction, this suspension was poured into a beaker containing 300 mL of 0.2 M hydrochloric acid solution under magnetic stirring for about 10 min. The foamed Si suspension was filtered and washed with distilled water several times. Finally, the foamed Si powder was obtained by drying at 60°C in a convection oven.

Materials characterization: The surface and cross-sectional morphology of the samples was observed by scanning electron microscopy (SEM, JEOL JSM-7000F). The samples for cross-sectional SEM analysis were prepared by cutting the particles using a cross-section polisher (JEOL IB09010CP). The microstructure of the particles was investigated by transmission electron microscopy (TEM, JEOL 2100F). The surface area and pore size were measured based on Brunauer-Emmett-Teller (BET) and Barrett-Joyner-Halenda (BJH) results using a surface analyzer (Micromeritics 3Flex). The crystal structure of the Si powders was characterized by X-ray (XRD) diffractometry (EMPYREAN PANanalytical) with Cu-K α radiation and Raman spectroscopy (JASCO NRS-3100). The surface of the Si powders was analyzed by Fourier transform infrared (FTIR) spectroscopy (Bruker VERTEX70) and X-ray photoelectron spectroscopy (XPS, Thermo Scientific Sigma Probe).

Electrochemical measurement: The electrochemical tests were performed using CR2032-type stainless coin cells with lithium metal as the counter and reference electrode. The working electrode was prepared by coating slurries on 10- μm -thick copper foil. The slurries were made by mixing the active material (Si powder, 60 wt%), conductive agent (Super-P, 20 wt%), and binder (polyacrylic acid, 20 wt%) in deionized water. The slurry-coated electrodes were dried at 120°C for 2 h under vacuum conditions and then allowed to naturally cool to room temperature. The loading of active materials in the electrode was 0.48 mg cm^{-2} . The coin cells were assembled in an Ar-filled glove box using a porous polyethylene membrane (Celgard 2400 membrane) as a separator and 1 mol L^{-1} LiPF_6 solution dissolved in a mixed solvent of ethylene carbonate (EC) and diethyl carbonate (DEC) (1:1 v/v), with additives of fluoroethylene carbonate (FEC, 10 wt%) and vinylene carbonate (VC, 5 wt%) (PANAX ETEC Co., Ltd.). Galvanostatic cycling measurements were carried out using a battery testing system at a current density of 200 mA g^{-1} for the ball-milled Si and 500 mA g^{-1} for the foamed Si electrodes in a voltage range of 0.005 to 1.5 V vs. Li/Li^+ (BaSyTec Cell Test System). The rate capability test of the foamed Si electrode was conducted in a voltage range of 0.005 to 1.5 V vs. Li/Li^+ at various current densities.

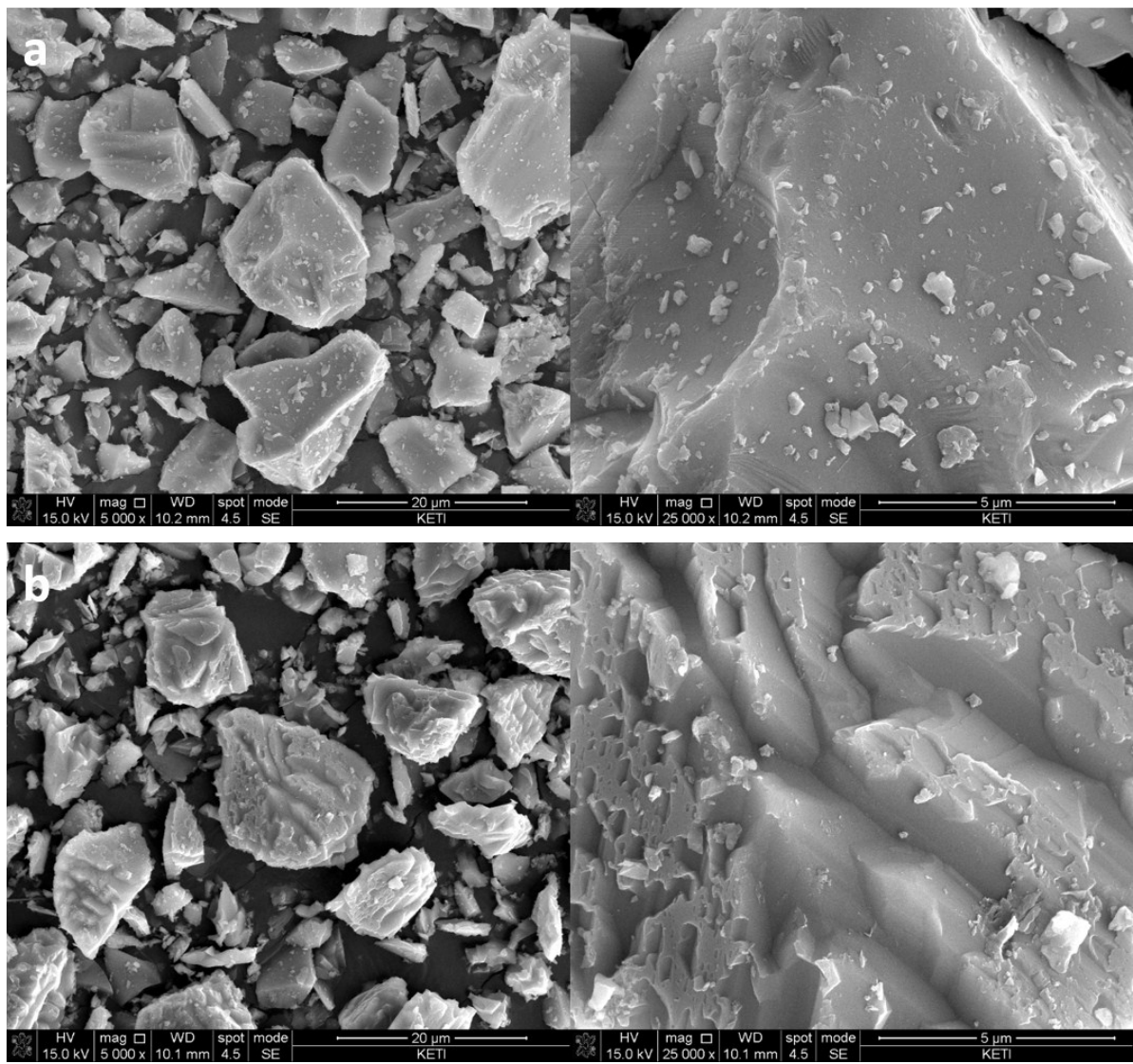


Fig. S1 SEM images of (a) bulk Si and (b) NaOH-treated bulk Si.

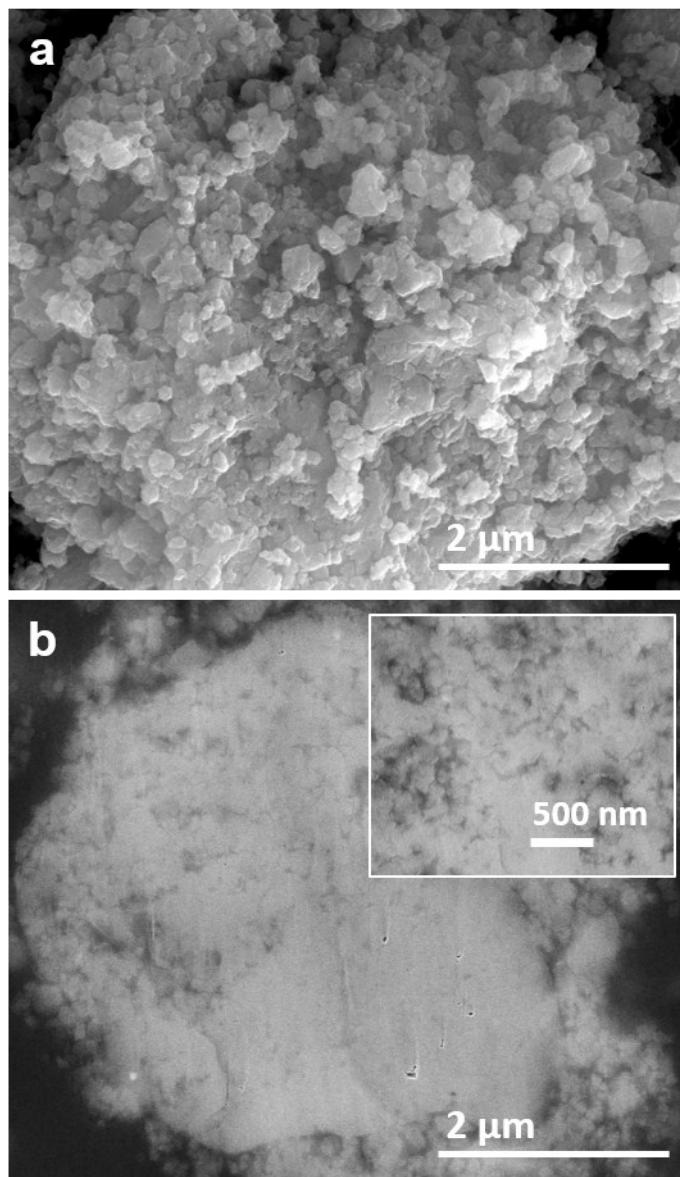


Fig. S2 (a) SEM image and (b) cross-sectional SEM image of ball-milled Si.

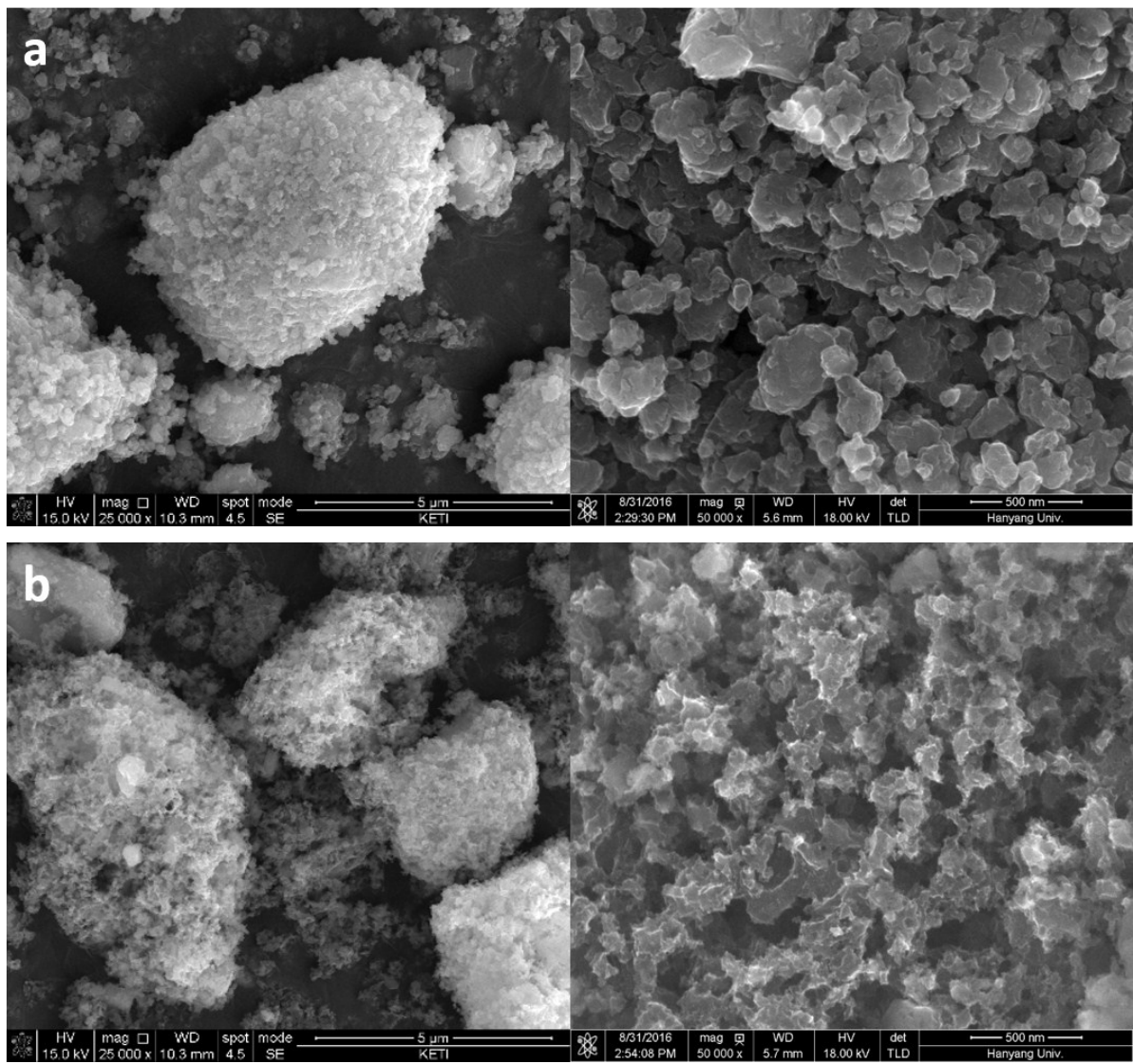


Fig. S3 Low (left side)- and high (right side)-magnification SEM images of (a) ball-milled Si particles and (b) foamed Si particles.

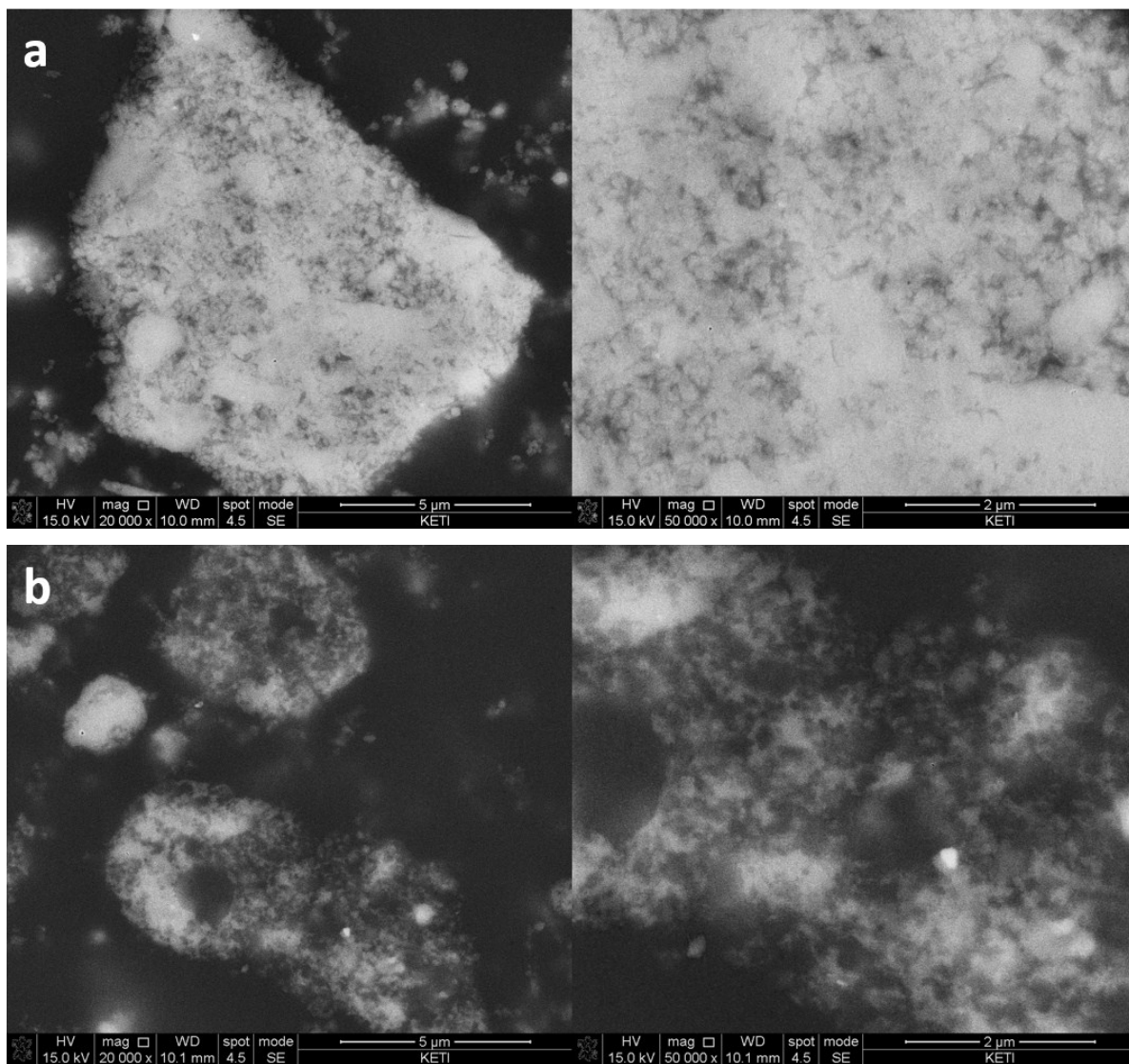


Fig. S4 Low (left side)- and high (right side)-magnification cross-sectional SEM images of (a) ball-milled Si particles and (b) foamed Si particles.

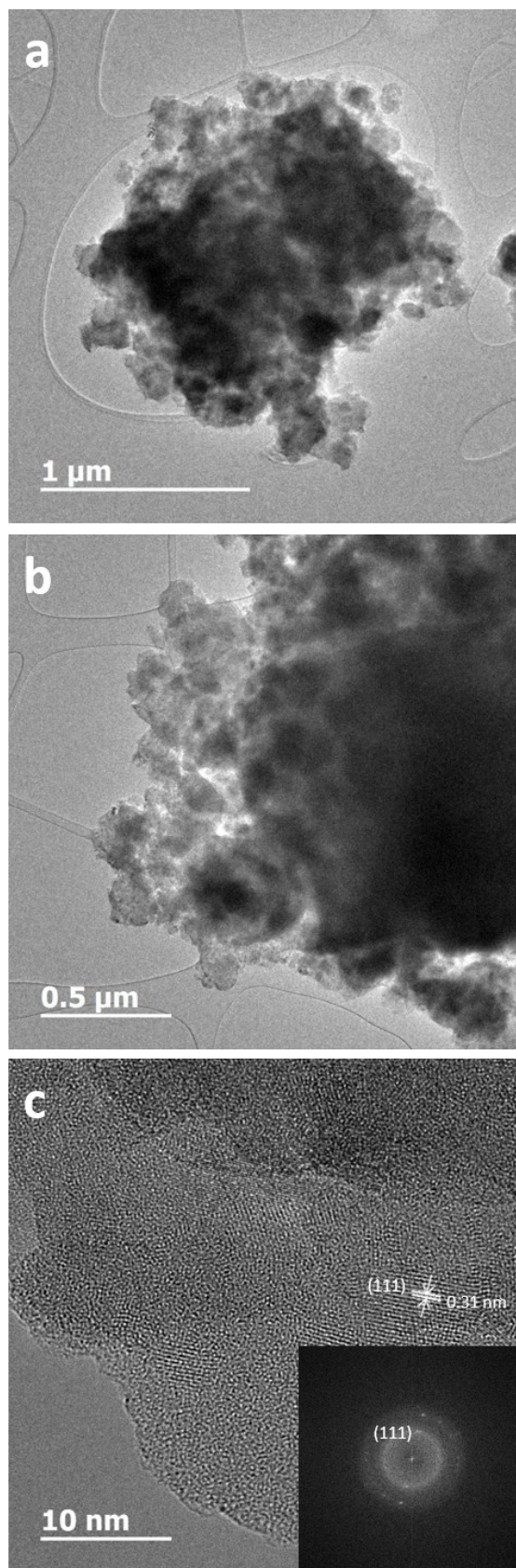


Fig. S5 (a),(b) TEM images of ball-milled Si particle. (c) HR-TEM image of ball-milled Si particle with FFT spots.

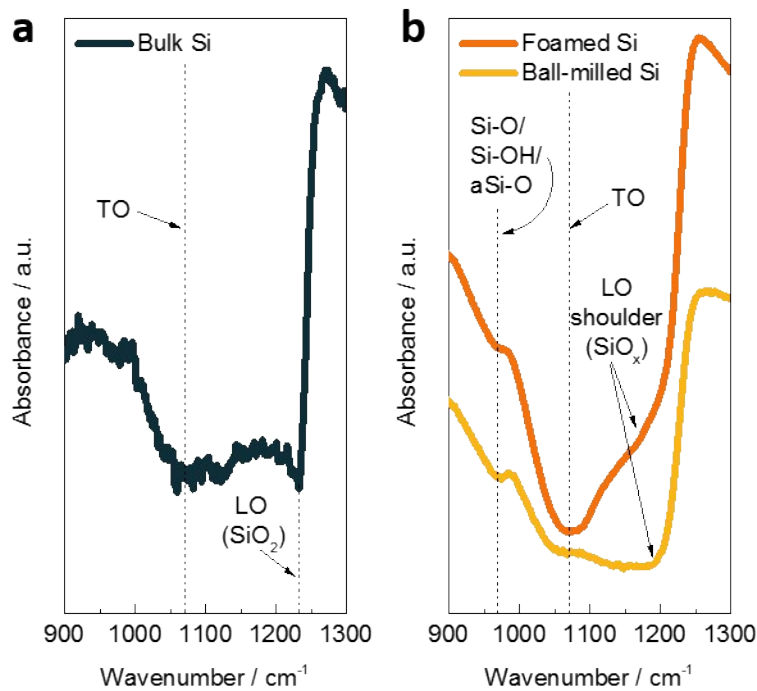


Fig. S6 FTIR spectra of (a) bulk Si, (b) ball-milled Si and foamed Si particles.

Fourier transform infrared spectroscopy (FTIR) spectra (Fig. S6) present the transverse-optical (TO) and longitudinal-optical (LO) split bands of the Si-O-Si asymmetric stretching mode.^{S1} A distinct sharp LO peak ($\sim 1230\text{ cm}^{-1}$) in the bulk Si (Fig. S6a) indicates the existence of a thin native SiO_2 layer on the surface of the Si powder.^{S1} On the other hand, the LO band of the ball-milled Si is located at a lower frequency of about 1200 cm^{-1} as a shoulder of the TO mode ($\sim 1070\text{ cm}^{-1}$) (Fig. S6b). Note that the distinguishable LO and TO bands in the SiO_2 merged into a single IR band in the non-stoichiometric SiO_x ($x < 2$).^{S2} Thus, the merged LO and TO bands observed in the FTIR spectra of the ball-milled Si (Fig. S6b) reveal that the newly evolved Si surface after ball milling was oxidized to non-stoichiometric SiO_x instead of SiO_2 by exposure to air at room temperature. The FTIR spectrum of the foamed Si also shows integrated Si-O-Si asymmetric stretching bands (Fig. S6b), which implies that the SiO_x on the surface of the ball-milled Si remained even after the etching process.

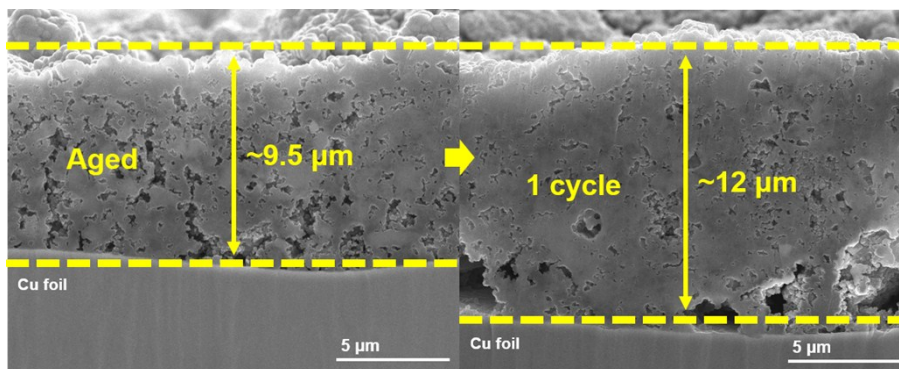


Fig. S7 Cross-sectional SEM images of the foamed Si electrode after aging (left) and 1 cycle (right).

Fig. S7 shows the cross-sectional SEM images of the foamed Si electrode before and after cycling. Compared with the aged electrode (left image of Fig. S7) for 24 h in the electrolyte, the cycled electrode (right image of Fig. S7) had slightly thicker active material layer. The thickness of aged and cycled electrodes were about 9.5 and 12 μm , respectively. Note that the initial reversible areal and specific volumetric discharge capacities were about 1.32 mAh cm^{-2} and 1390 mAh cm^{-3} , respectively. The foamed Si electrode showed high integrity of active materials against huge volume changes of Si during cycling, which might be due to the interconnected submicron sized Si network that prevents detachment of active Si parts. Although the structure integrity of foamed Si electrode was stable (Fig. S7), the foamed Si electrode showed a gradual decrease of discharge capacity with the increase of cycles (Fig. 4d). This might be due to the continuous solid electrolyte interphase (SEI) film formation on the newly exposed Si surface after charge and discharge process, increasing the impedance of the electrode.^{S3}

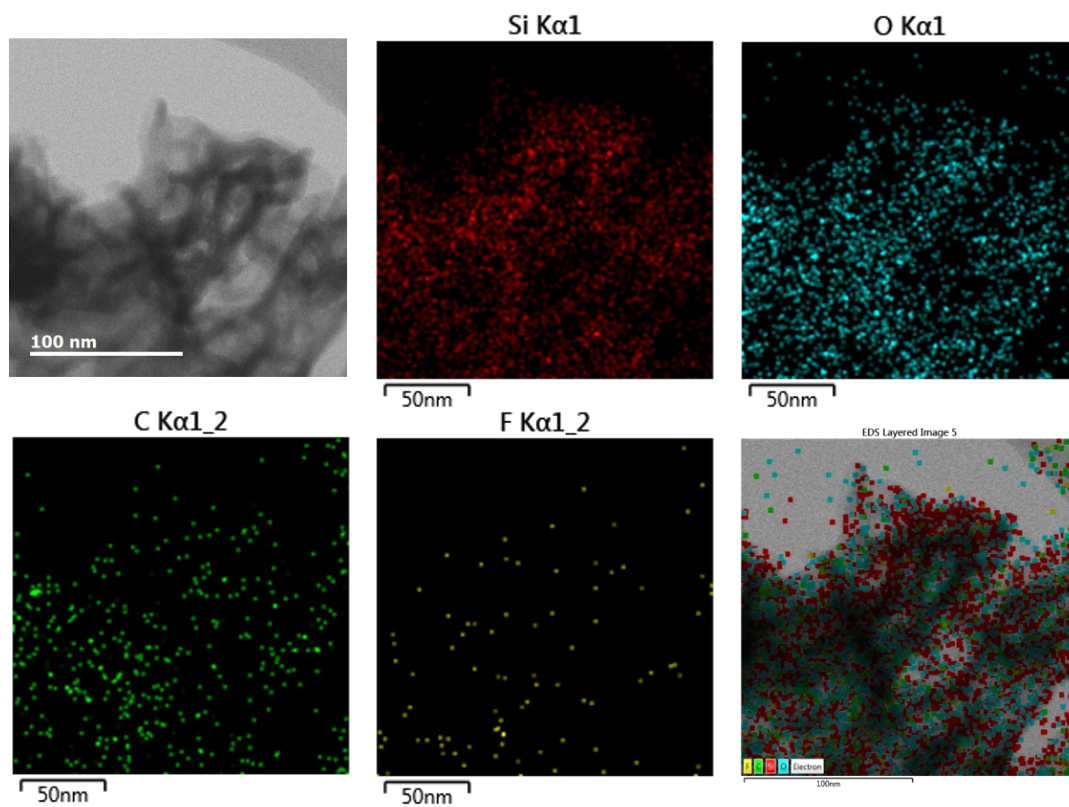


Fig. S8 EDS mapping of a cycled foamed Si particle.

Table S1. BET and BJH data of bulk Si, ball-milled Si and foamed Si particles.

	Bulk Si	Ball-milled Si	Foamed Si
BET surface area [m ² g ⁻¹]	0.8173	14.6345	23.3675
BJH Adsorption cumulative volume of pores between 17.000 Å and 3,000.000 Å diameter [cm ³ g ⁻¹]	-	0.082548	0.133413
BJH Desorption cumulative volume of pores between 17.000 Å and 3,000.000 Å diameter [cm ³ g ⁻¹]	-	0.083695	0.134641
BJH Adsorption average pore diameter [nm]	-	39.4422	45.2832
BJH Desorption average pore diameter [nm]	-	29.8677	38.3226

Table S2. Ratios of XRD peak intensities with respect to (111) peak intensity for bulk, ball-milled and foamed Si particles.

	(111)/(111)	(220)/(111)	(311)/(111)	(400)/(111)	(331)/(111)	(422)/(111)
Bulk Si	1	0.58	0.29	0.06	0.11	0.14
Ball-milled Si	1	0.45	0.22	0.05	0.07	0.08
Foamed Si	1	0.52	0.29	0.07	0.1	0.12

Table S3. XPS data for surficial composition of bulk, ball-milled and foamed Si particles.

	S2p	O1s	Fe2p	Na1s
	[at%]	[at%]	[at%]	[at%]
Bulk Si	53.79	46.07	0.01	0.13
Ball-milled Si	57.63	42.29	0.01	0.07
Foamed Si	52.06	47.37	0.52	0.08

References

- S1. (a) P. Innocenzi, *J. Non-Cryst. Solids*, 2003, **316**, 309-319; (b) K. T. Queeney, H. Fukidome, E. E. Chaban and Y. J. Chabal, *J. Phys. Chem. B*, 2001, **105**, 3903-3907; (c) A. Demšar, B. Colarič, S. Rus., J. Lindav, F. Švegelj, B. Orel, B. Praček and A. Zalar, *Thin Solid Films*, 1996, **281-282**, 409-411.
- S2. (a) P. G. Pai, S. S. Chao, Y. Takagi and G. Lucovsky, *J. Vac. Sci. Technol. A*, 1986, **4**, 689-694; (b) C. Songyan, P. K. Kashkarov, V. Y. Timoshenko, L. Baolin and J. Bingxi, *J. Cryst. Growth*, 2003, **247**, 445-451; (c) K. Furukawa, Y. Liu, D. Gao, H. Nakashima, K. Uchino and K. Muraika, *Appl. Surf. Sci.*, 1997, **121/122**, 228-232.
- S3. (a) E. Radvanyi, K. V. Havenbergh, W. Porcher, S. Jouanneau, J.-S. Bridel, S. Put, S. Franger, *Electrochim. Acta*, 2014, **137**, 751-757; (b) J. Zheng, H. Zheng, R. Wang, L. Ben, W. Lu, L. Chen, L. Chen and H. Li, *Phys. Chem. Chem. Phys.*, 2014, **16**, 13229-13238; (c) M. Ashuri, Q. He and L. L. Shaw, *Nanoscale*, 2016, **8**, 74-103; (d) Y. Oumellal, N. Delpuech, D. Mazouzi, N. Dupré, J. Gaubicher, P. Moreau, P. Soudan, B. Lestriez and D. Guyomard, *J. Mater. Chem.*, 2011, **21**, 6201-6208.